Catalysis Science & Technology

Accepted Manuscript

This is an *Accepted Manuscript*, which has been through the Royal Society of Chemistry peer review process and has been accepted for publication.

Accepted Manuscripts are published online shortly after acceptance, before technical editing, formatting and proof reading. Using this free service, authors can make their results available to the community, in citable form, before we publish the edited article. We will replace this *Accepted Manuscript* with the edited and formatted *Advance Article* as soon as it is available.

You can find more information about *Accepted Manuscripts* in the Information for Authors.

Please note that technical editing may introduce minor changes to the text and/or graphics, which may alter content. The journal's standard Terms & Conditions and the Ethical guidelines still apply. In no event shall the Royal Society of Chemistry be held responsible for any errors or omissions in this *Accepted Manuscript* or any consequences arising from the use of any information it contains.

ROYAL SOCIETY OF CHEMISTRY

www.rsc.org/catalysis

Yttrium oxide modified $Cu/ZnO/Al_2O_3$ catalysts via hydrotalcite-like precursors for the CO_2 hydrogenation reaction to methanol

Peng Gao [a,b,*], Liangshu Zhong [a], Lina Zhang [c], Hui Wang [a,b], Ning Zhao [c], Wei Wei [a,b], Yuhan Sun [a,c,*]

[a] CAS Key Lab of Low-Carbon Conversion Science and Engineering, [b] Center for Greenhouse Gas and Environmental Engineering, Shanghai Advanced Research Institute, Chinese Academy of Sciences, No.99 Haike Road, Zhangjiang Hi–Tech Park, Shanghai 201203, China

[c] State Key Laboratory of Coal Conversion, Institute of Coal Chemistry, Chinese Academy of Sciences, Taiyuan 030001, China

* Corresponding author. Tel: +86–021–20608001, Fax: +86–021–20608001.

E–mail: gaopeng@sari.ac.cn (P. Gao), sunyh@sari.ac.cn (Y.H. Sun)

Abstract: Y_2O_3-modified $Cu/ZnO/Al_2O_3$ catalysts (Cu^{2+}:Zn^{2+}:(Al^{3+}+Y^{3+}) = 2:1:1) via hydrotalcite-like precursors were synthesized with Y^{3+}:(Al^{3+}+Y^{3+}) atomic ratios between 0 and 0.5. With the introduction of certain amount of Y_2O_3, the surface area and dispersion of Cu for $Cu/ZnO/Al_2O_3$ catalysts increased significantly. However, excess Y_2O_3 content would decrease the dispersions of both Cu and ZnO as a result of the declined amount of hydrotalcite-like phases in the precursor. It was suggested that Y_2O_3 and the hydrotalcite-like structure could prevent the aggregation of Cu nanoparticles during reduction and reaction process and improve the reducibility of Cu^{2+} species. As Cu^0 species were predominant active sites for the methanol synthesis from CO_2 hydrogenation, addition of suitable amount of Y_2O_3 to $Cu/ZnO/Al_2O_3$ catalyst enhanced the catalysis for CO_2 hydrogenation remarkably. Nevertheless, the CO_2 conversion decreased significantly when Y^{3+}:(Al^{3+}+Y^{3+}) > 0.1 due to the lower Cu surface area and a relatively weaker interaction between Cu and ZnO. The $Cu/ZnO/Al_2O_3/Y_2O_3$ catalyst with Y^{3+}:(Al^{3+}+Y^{3+}) = 0.1 derived from hydrotalcite-like compounds afforded the best catalytic performance with high stability.

Catalysis Science & Technology Accepted Manuscript

Keywords: Yttrium oxide; Hydrotalcite-like structure; CO_2 hydrogenation; Methanol synthesis; $Cu/ZnO/Al_2O_3$ catalyst

1. Introduction

The transformation of CO_2 into valuable chemicals and fuels is a promising route that may offer a solution to control greenhouse gas and substitute dwindling fossil fuels.[1,2] Among the many options considered, catalytic conversion of CO_2 to methanol has attracted widely attention because methanol is an important raw material in the chemical industry and can be used directly as clean fuel.[2-4] In addition, high-octane gasoline, aromatics, ethylene, as well as many other value-added petrochemicals, which now are mainly derived from crude oil, can also be produced from methanol. In order to realize a green integrated process for CO_2 hydrogenation to methanol, the needed hydrogen can be generated from natural gas, shale gas, and other methane sources or water electrolysis, and CO_2 capture and recycling can use any available alternative energy.[3, 5]

$Cu/ZnO/Al_2O_3$ catalysts, conventionally used for commercial synthesis of methanol from CO_2-containing syngas, are also widely investigated for the methanol synthesis from CO_2 hydrogenation.[6-11] However, the low activity and stability of $Cu/ZnO/Al_2O_3$ catalysts, which is partly ascribed to Cu sintering accelerated by the presence of water vapor byproduct, create major barriers toward direct application for CO_2 hydrogenation.[12-14] For Cu-based catalysts, many researchers found that the Cu surface area and Cu dispersion were mainly responsible for the catalytic performance and there was a linear relationship between the activity and Cu surface area.[15-19] Other researchers reported that the catalytic activity increased with increasing Cu surface area and/or Cu dispersion, but it was not a linear relationship.[10, 20, 21] In addition, the performance for CO_2 hydrogenation to methanol was also related to the reducibility of CuO, the synergy between Cu and oxide, and the surface basicity of catalysts.[16, 20-24] Moreover, some literatures pointed out that both Cu^0 and Cu^+ species were essential to catalyze the CO_2 hydrogenation to methanol and the stabilization of the Cu^+ ions

Catalysis Science & Technology Accepted Manuscript

favored the hydrogenation of CO_2.[25-27]

Detailed studies on the phase structure of the Cu-containing hydroxocarbonates precipitate revealed that the precipitate phases played an important role for the structure and performance of catalysts.[28, 29] It was suggested that the topotactic nature of the hydrotalcite-like compounds (HTlcs) decomposition to metal oxide could induce the formation of nanocatalysts with homogeneous dispersion of metal cations at atomic level, strong synergetic effects among different components, high specific surface area, strong basic properties and high stability against sintering.[30-32] Several studies on Cu-containing hydrotalcite-like (HTl) precursors have also proven the advantages of HTl phases as precursors for Cu-based catalysts in various reactions.[30-33] Therefore, it is expected that using HTlcs as precursors for the $Cu/ZnO/Al_2O_3$ catalyst would promote the catalytic activity and stability for the CO_2 hydrogenation reaction to methanol. To further improve the catalysis of the $Cu/ZnO/Al_2O_3$ catalyst, an effective promoter is needed. Among the promoters studied, yttrium oxide is a very promising candidate because the introduction of Y_2O_3 into Cu-based catalyst can increase Cu specific surface area significantly.[12, 34, 35] In our previous work, the influence of several modifiers (Mn, La, Ce, Zr and Y) on the properties of $Cu/ZnO/Al_2O_3$ catalysts was investigated and it was found that the Y_2O_3-modified catalyst exhibited the highest CO_2 conversion with the maximum of Cu surface area and Cu dispersion compared with other additives.[18] However, a comprehensive study of the influence of Y_2O_3 on the methanol synthesis catalysts is – to the best of our knowledge – still lacking.

In the present study, a series of Y_2O_3-modified $Cu/ZnO/Al_2O_3$ catalysts (Cu^{2+}:Zn^{2+}:(Al^{3+}+Y^{3+}) = 2:1:1) derived from HTl precursors were synthesized with Y^{3+}:(Al^{3+}+Y^{3+}) atomic ratios between 0 and 0.5 and were evaluated for methanol synthesis from CO_2 hydrogenation. In order to better understand and design the highly active catalysts for CO_2 hydrogenation to methanol, the active state of copper was clarified by *in situ* XRD and *ex situ* XPS during reduction process. The relationships among the precursor structure, the physicochemical properties of catalysts, as well as the catalytic activity and stability were investigated in detail. In addition, the

Catalysis Science & Technology Accepted Manuscript

promoting effects of Y_2O_3 on properties and catalytic performance of the $Cu/ZnO/Al_2O_3$ catalysts were studied based on structure−activity relationships.

2. Experimental

2.1. Preparation of Catalysts

Cu/Zn/Al/Y hydrotalcite-like compounds (Cu^{2+}:Zn^{2+}:(Al^{3+}+Y^{3+}) = 2:1:1) were synthesized with atomic ratios of Y^{3+}:(Al^{3+}+Y^{3+}) = 0, 0.05, 0.1, 0.2 and 0.5, respectively. All the precursors were obtained by co-precipitation method at 293 K, using "pro analyze" purity grade nitrate salts of the corresponding metals ($Cu(NO_3)_2{\cdot}3H_2O$, $Zn(NO_3)_2{\cdot}6H_2O$, $Al(NO_3)_3{\cdot}9H_2O$ and $Y(NO_3)_3{\cdot}6H_2O$), and a mixed solution of NaOH and Na_2CO_3 as precipitation agent. Typically, the mixed Cu/Zn/Al/Y solution and the precipitant were added dropwise to 200 mL of deionized water under vigorous stirring. The pH during precipitation was kept at a constant value of 10.0 ± 0.2. The product was aged at 333 K for 15 h under stirring and then filtered and washed with deionized water. Finally, the filter cakes were dried overnight at 353 K and further calcined in air at 773 K for 4 h. The as-obtained HTlcs were denoted as HT-Y*x* (*x* is the Y^{3+}:(Al^{3+}+Y^{3+}) atomic ratio in the synthesis mixture), and the corresponding calcined HTlcs were denoted as CHT-Y*x*.

2.2. Characterization of Catalysts

The surface area of samples was determined by N_2 adsorption–desorption at liquid nitrogen temperature 77.30 K, using a Micromeritics Tristar 3000 instrument. Sample degassing was carried out at 473 K prior to acquiring the adsorption isotherm.

Elemental chemical analysis was performed using the inductively coupled plasma–optical (ICP) emission spectroscopy (Thermo iCAP 6300).

Powder X–ray diffraction (XRD) patterns were recorded on a Panalytical X'Pert Pro Super X–ray diffractometer with Cu Kα radiation (λ= 0.15418 nm), in the step mode (0.0167°, 12 s) and in the range of 5° < 2θ < 75°. The full width at half maximum (FWHM) of Cu (1 1 1) diffraction at a 2θ of 43.2° was used to calculate the mean crystallite size of Cu using the Scherrer equation. For *in situ* XRD measurement,

Catalysis Science & Technology Accepted Manuscript

the sample remained in 5% H_2/He mixture at a flow rate of 50 mL min^{-1}. Temperature ramping programs were performed from 298 K to 448, 473, 498, 523, 573, 623, and 673 K at a heating rate of 5 K min^{-1}. The XRD patterns were collected after samples reached the preset temperatures for 30 min. For another *in situ* XRD measurement, the sample also remained in 5% H_2/He mixture, and temperature ramping programs were performed from 448 K to 473, 498, 523, 548, and 573 K at a heating rate of 5 K min^{-1}. The XRD patterns were collected once samples reached the preset temperatures.

Thermal decomposition of the catalyst precursors was studied by thermogravimetric (TG) method by using SDT-Q600 Thermal Analyzer. Measurements were performed in the temperature range of 303–1023 K with linear temperature program β = 10 K min^{-1} in continuous flow of synthetic air (30 mL min^{-1}).

Transmission electron microscope (TEM) and high resolution transmission electron microscope (HRTEM) were performed on an FEI Tecnai F20 transmission electron microscope with a field emission gun operating at 200 kV to investigate the dimensions and the structural details of the samples after different treatments.

The dispersion of Cu (D_{Cu}) and exposed Cu surface area (S_{Cu}) were determined by dissociative N_2O adsorption and carried out on Micromeritics AutoChem 2920 instrument using the procedure described in our previous work.[18] Before measurements the catalysts (0.1 g) were reduced at 573 K in 5% H_2/Ar mixture (30 mL min^{-1}) for 2 h. Then, the sample was exposed to N_2O (85 mL min^{-1}) for 1 h to ensure complete oxidation of surface metallic copper. Finally, a pulse of pure H_2 was passed over the catalyst at 573 K and the surface Cu_2O were reduced in the pulse of pure H_2. D_{Cu} and S_{Cu} were calculated from the amount of hydrogen consumption. In addition, the average Cu particle size (d_{Cu}) obtained from the conventional formula

$$d_{Cu}(nm) = \frac{104}{D_{Cu}(\%)} \quad (1)$$

assuming a spherical shape of Cu particles.[21]

X–ray photoelectron spectroscopy (XPS) and Auger electron spectroscopy (XAES)

Catalysis Science & Technology Accepted Manuscript

were performed over a Quantum 2000 Scanning ESCA Microprobe instrument equipped with Al *K*α radiation (15 kV, 25 W, *hv* = 1486.6 eV) under ultrahigh vacuum (10^{-7} Pa). Prior to each test, the calcined sample was reduced in pure hydrogen at 573 K for 8 h, and the XPS measurements were recorded with the exclusion of air contact after reduction. The binding energies were calibrated internally by adventitious carbon deposit C (1s) with E_b = 284.6 eV (accuracy within ±0.1 eV).

Temperature program reduction (TPR) was carried out in a U-tube quartz reactor. The samples (50 mg) were purged with Ar (30 mL min^{-1}) at 423 K to remove physically adsorbed water and then reduced in a flow of 5 vol% H_2 + Ar (30 mL min^{-1}) at a heating rate of 5 K min^{-1} up to 873 K. Thermal conductivity detector (TCD) was used to monitor the consumption of H_2.

H_2 temperature programmed desorption (H_2–TPD) was carried out in the range 323–923 K with a heating rate of 10 K min^{-1} using Ar as carrier gas (40 mL min^{-1}). Prior to the adsorption of H_2, the catalyst was first reduced at 573 K in H_2 flow of 30 mL min^{-1} for 2 h. After cooling to room temperature, the catalyst was saturated with pure H_2 (30 mL min^{-1}) at 323 K for 60 min and then flushed with Ar flow (40 mL min^{-1}) to remove all physical adsorbed molecules. The desorption process was monitored by a TCD quantitatively calibrated by H_2 pulses.

2.3. Evaluation of Catalysts

CO_2 hydrogenation to methanol was evaluated in a continuous fixed-bed stainless steel reactor. The catalyst (0.6 g, 40–60 mesh) diluted with quartz sand (40–60 mesh) was placed in a stainless steel tube reactor. Prior to reaction, the catalyst was firstly pre-reduced at 573 K and atmospheric pressure for 6 h by a pure hydrogen stream (80 mL min^{-1}) and then cooled to room temperature. After reduction, the activities of the catalysts were determined under flow of H_2, CO_2 and N_2 mixture ($H_2/CO_2/N_2$ molar ratio of 73/24/3). The products were quantitative analyzed with a Shimadzu GC-2010C gas chromatograph equipped with a thermal conductivity detector (TCD, TDX-01 column) for gas of H_2, N_2, CO, CH_4 and CO_2, and Propark-Q for liquid of H_2O and CH_3OH. The CO_2 conversion and the carbon-based selectivity for CH_3OH,

Catalysis Science & Technology Accepted Manuscript

CH_4 and CO were calculated by an internal normalization method. The space time yield (STY) of CH_3OH, which gave the amounts of CH_3OH produced per gram catalyst per hour, was defined as the Eq (2):

$$STY_{CH_3OH} = \frac{W_T \times X(CH_3OH)}{t \times m} \quad (2)$$

where W_T was the total weight of CH_3OH and H_2O product (g); $X(CH_3OH)$ was the mass fraction of CH_3OH; t was the reaction time (h); m was the weight of catalyst (g). Each data set was obtained from an average of three independent measurements.

3. Results and discussion

3.1. Textural and structural properties of the precursors

Powder X-ray diffraction patterns of the uncalcined precursors are shown in Fig. 1. The peaks at 2θ of 12°, 24°, and 35 ° were attributed to the (0 0 3), (0 0 6), and (0 0 9) crystal planes in the layered structure with rhombohedral symmetry (3R). In addition, the broad and asymmetric peaks at 36 °, 39 °, and 47 ° were ascribed to the (0 1 2), (0 1 5), and (0 1 8) crystal planes, respectively. For the samples of HT-Y0, HT-Y0.05 and HT-Y0.1, the well-defined (1 1 0) and (1 1 3) diffraction peaks were also observed at 60 ° and 61 °, indicating a homogeneous dispersion of various cations in the hydroxide layers.[36] No other crystalline phases were observed. However, the crystallinity of the samples decreased with the increasing Y^{3+}:(Al^{3+}+Y^{3+}) ratio which was probably due to the introduction of large distortions in the hydrotalcite-like (HTl) layers as a result of the substitution of Al^{3+} (ionic radius 0.053 nm) by the much larger ionic radius Y^{3+} (0.090 nm),[37] and the coformation of amorphous precipitate (such as hydroxides and hydroxyl carbonates).[38, 39] High Al content favors the formation of hydrotalcite-like compounds (HTlcs), therefore, the yields of HTl phase in precursors may decrease with increase of Y content.[23, 29]

The calculated lattice parameters of the prepared HTlcs are listed in Table 1. The increase of Y^{3+}:(Al^{3+}+Y^{3+}) ratio provokes the increase of the lattice parameters a and c. The increase of the lattice parameters a (= $2d_{1\,1\,0}$), which is a function of the average radius of the metal cations in the layers,[40] can be assigned to the substitution

Catalysis Science & Technology Accepted Manuscript

of the smaller radius of Al^{3+} by the larger radius of Y^{3+} in the layers. The increase in parameters c (= $d_{003}+2d_{006}+3d_{009}$), which is a measure of the thickness of the HTl layer and the interlayer distance, is attributed to the lower polarizing ability of Y^{3+} compared to Al^{3+}, thus decreasing the Coulombic attractive force between the positively charged HTl layers and the negatively charged interlayer anions.[37] Another probable reason is that some added Y^{3+} ions are present at the corners of the hexagonal crystal lattice, causing a sharp increase in the thickness of the HTl layer.[38] It is also found that c should increase with incorporation of any amount of Y^{3+} into the layer, but without changing appreciably as more and more yttrium is present in the layer.

The TG profiles for various precursors are shown in Fig. 2. In general, the thermal decomposition (weight loss) of the Cu-containing HTlcs consists of three steps, namely, dehydration of physically adsorbed and interlayer water molecules at 373-473 K, dehydroxylation of the HTl layer and loss of carbonate anions of the interlayer space at 473-823 K, and the decomposition of Cu oxocarbonates formed during the former steps of the thermal decomposition of the HTl structure above 823 K.[33, 41] The second step resulted in the collapse of the layered structure and the weight loss at this step may also be due to the decomposition of amorphous hydroxycarbonates.[38]

The weight losses measured in TG experiments for all steps are compared in Table 1. The Y-containing samples lost about 9% more than the Y-free sample, suggesting that the amount of H_2O and CO_2 from the decomposition of precursors increased with the introduction of Y^{3+}. With increasing content of Y^{3+} in precursors, the second weight loss due to the decomposition of the HTl species and amorphous hydroxycarbonates increased, while the amount of Cu oxocarbonates (the third weight loss) formed during decomposition of the HTl structure decreased, which revealed that the higher Y^{3+}:(Al^{3+}+Y^{3+}) atomic ratio in the mother liquid, the less HTl phases and the more amorphous phases existed in the precursor, in agreement with the XRD results of the precursors.

Fig. 2 also shows that all the weight losses are recorded at lower temperatures with the introduction of Y^{3+}, indicating the decrease of the thermal stability for

Catalysis Science & Technology Accepted Manuscript

Cu/Zn/Al/Y precursors. As mentioned above, the introduction of Y^{3+} cations would reduce the Coulombic interaction between the layers and the interlayer anions, leading to lower thermal stability. In addition, the removal of molecular water at lower temperature can be related to the lower charge-to-size ratio for Y^{3+} than for Al^{3+}. However, with further increasing Y content, the weight losses occurred at higher temperatures, which can be related to the decreased amount of HTl phases.

3.2. Textural and structural properties of the calcined samples

The XRD patterns of derived oxides (Fig. 3a) show the complete transformation from the HTl phase to the oxide phase after calcination at 773 K. Some broad diffraction peaks for a poorly crystallized CuO phase are detectable for all the samples while no diffraction peaks belonging to Al_2O_3 and Y_2O_3 are found. In addition, the poorly crystallized ZnO phase is observed only for the sample CHT-Y0.5. The metal compositions of calcined CHT-Y*x* samples measured by ICP are presented in Table 2. The compositions of the catalysts were in close agreement with the nominal compositions taken for the catalysts preparations, suggesting the complete precipitation of the metallic nitrates. It can be noted that both the Cu^{2+}:Zn^{2+} and Y^{3+}:(Al^{3+}+Y^{3+}) ratios results were close to those used in the starting solutions.

Ex situ XRD patterns of the CHT-Y*x* catalysts after reduction at 573 K for 6 h are shown in Fig 3b. To prevent and diminish phase transformation that probably occurred during exposure to air, the reduced samples were carefully collected and preserved in liquid paraffin at room temperature and sealed into glass bottles before XRD analysis. For all the samples, the broad and diffuse peak at around 18.2 ^{o} was attributed to paraffin. Upon reduction at 573 K, the XRD diffraction peaks (2θ = 35.6 ^{o} and 38.8 ^{o}) of CuO disappeared, while the peaks (2θ = 43.2 ^{o}, 50.2 ^{o}, and 74.1 ^{o}) attributed to metallic Cu emerged in these catalysts. In addition, the intensity of the metallic Cu diffraction peak declined markedly with the introduction of Y^{3+}. For the sample CHT-Y0.5, the diffraction peaks (2θ = 31.9 ^{o}, 34.4 ^{o}, and 36.1 ^{o}) of ZnO could be clearly seen after reduction, indicating that the dispersion of ZnO in reduced CHT-Y0.5 was much lower,[42, 43] which might be related to the decreasing amount of

Catalysis Science & Technology Accepted Manuscript

HTl phases with increased Y content. The Cu crystallite size (d_{Cu}) calculated by the Scherrer equation decreased markedly with increasing Y content, while the average Cu particle size increased slightly when Y^{3+}:(Al^{3+}+Y^{3+}) > 0.1, and the minimum d_{Cu} was 8.3 nm for CHT-Y0.1 (Table 2). A similar trend for Cu particle size determined by dissociative N_2O adsorption was also found from Table 2. These results clearly demonstrated that the incorporation of the suitable amount of Y_2O_3 hindered the growth of Cu particle size upon heat treatment. Moreover, ZnO acts as a physical spacer between Cu nanoparticles and helps disperse the Cu phase.[24, 44] With the addition of excess of Y, the amount of HTl phased in the precursor decreased and led to a lower dispersion of ZnO. As a result, d_{Cu} increased with further increase of Y content.

The *in situ* XRD characterization was adopted to further explore the phase evolution of representative CHT-Y0, CHT-Y0.1 and CHT-Y0.5 under 5% H_2/95%He as a function of reduction temperature. For the CHT-Y0 sample (Fig. S1 in the Supplementary material), the diffraction peaks (2θ = 35.5 ^{o} and 38.9 ^{o}) of CuO can be observed at 298 K. The CuO peaks disappeared and the characteristic peaks of Cu at 2θ of 43.2 ^{o}, 50.2 ^{o}, and 74.1 ^{o} became observable with the increasing temperature to 498 K. Continuous increasing the reduction temperature inevitably caused the sintering and aggregation of metallic copper particles, as evidenced by the gradual sharpening of metallic Cu characteristic peaks. In addition, the very weak peaks (2θ = 31.9 ^{o}, 34.4 ^{o}, and 36.1 ^{o}) of ZnO appeared when the reduction temperature rising to 673 K. The mean copper particle size calculated by the Scherrer equation remarkably grew up from 9.3 to 16.4 nm when the reduction temperature enhanced from 498 to 673 K. Similar trend of phase evolution has been observed for CHT-Y0.1 (Fig. S2) and CHT-Y0.5 samples (Fig. S3), while the characteristic peaks of Cu became detectable at lower temperature 473 K compared to CHT-Y0. For CHT-Y0.5, the phase's crystallinity of ZnO increased markedly with increase of reduction temperature. However, with the introduction of Y^{3+}, the average copper particle size for the CHT-Y0.1 sample grew moderately from 6.4 to 7.3 nm with increasing temperature from 498 to 673 K. Moreover, the increase of copper particle size for

Catalysis Science & Technology Accepted Manuscript

CHT-Y0.5, which increased from 6.5 to 10.5 nm under the same condition, also became obvious with further increase of Y content, which might be related to the lower dispersion of ZnO as a result of the decreased amount of HTl phases with increase of Y content. Therefore, we deduced that the incorporation of Y_2O_3 and the HTl structure were capable of immobilizing copper species and suppressing sintering of copper particles during the calcination and reduction. Moreover, the *in situ* XRD patterns were collected once samples reached the preset temperatures, and the diffraction peaks of Cu_2O (2θ = 36.4 ^{o}) could be observed during the heating of CHT-Y0, CHT-Y0.1 and CHT-Y0.5 in 5% H_2/He from 448 to 573 K at a heating rate of 5 K min^{-1}. For CHT-Y0, both Cu_2O and Cu peaks appeared when the reduction temperature rising to 548 K (Fig. S4), while these peaks were observed at lower temperature for CHT-Y0.1 (498 K) and CHT-Y0.5 (523 K) samples (Fig. S5 and S6), and the peaks of Cu_2O disappeared with further increase of temperature. Especially for CHT-0.1, three kinds of copper species (CuO, Cu_2O and Cu) can be found when the temperature enhanced to 498 K (Fig. S5). These results suggested that the reduction of CuO to metallic Cu passed through an intermediate Cu_2O phase which was very unstable and easily and quickly reduced to metallic Cu under H_2 atmospheres.

The transmission electron microscopy (TEM) and high resolution transmission electron microscopy (HRTEM) images illustrate the typical microstructure of the CHT-Y*x* catalysts after different treatments. It can be seen from Fig. S7 that the calcined samples were composed of platelet-like particles, which indicated that the derived oxides remained the morphological characteristic of HTl precursors. The pretended needle-like morphology of the calcined particles was corresponding to projections of platelets (Fig. S7). For CHT-Y0.5, a large amount of spherically shaped particles were observed, and minor amounts of plate-like particles could be found (Fig. S7c). After reduction of CHT-Y0 and CHT-Y0.1 catalysts at 573 K for 6 h, the samples still maintained the overall plate-like morphology (Fig. $4a_1$ and $4b_1$). However, the surface turned to rough and abundant dispersed small dots were observed throughout the platelets. On the lamellar plates of reduced CHT-Y0 and

Catalysis Science & Technology Accepted Manuscript

CHT-Y0.1 samples, spherically shaped and well crystalline of Cu could be noticed from HRTEM images and no indication for individual separated oxide particles were found (Fig. $4a_2$ and $4b_2$). In addition, the Cu particles were partly embedded in the remaining metal oxide matrix resulting in an intimate interface contact of Cu particles and continuous Cu depleted oxide. The major part of the reduced CHT-Y0.5 sample comprised the compact particles (Fig. $4c_1$). Apart from Cu particles, the separated ZnO particles were also observed from Fig. $4c_2$. Therefore, it can be speculated that the interaction among Cu and ZnO for CHT-Y0 and CHT-Y0.1 was stronger than that for CHT-Y0.5. The average diameter of Cu particles for CHT-Y0 was around 10–15 nm and it decreased below 10 nm with the introduction of Y_2O_3 for CHT-Y0.1 and CHT-Y0.5, in agreement with the results from XRD and N_2O chemisorption analysis (Table 2). Furthermore, Fig. S8 also shows the TEM images of the spent CHT-Y0, CHT-Y0.1 and CHT-Y0.5 catalysts after stability test. Some lamellar plates were decomposed and more agglomerated particles on the platelets could be found after 500 h reaction.

The textural properties of CHT-Y*x* samples with different Y content are summarized in Table 2. It can be found that the BET specific surface areas (S_{BET}) of Y_2O_3-modified catalysts were much higher than that of the Y_2O_3-free sample, and the values increased significantly with increase of Y content until they reached the maximum for CHT-Y0.1 and CHT-Y0.2 samples and then decreased slightly. These results were mainly related to the amount of H_2O and CO_2 evolved from the precursors during the second weight loss, according to the TG analysis. In addition, the pore volume increased gradually with increasing Y content. The reactive N_2O adsorption on reduced samples (Table 2) was to determine the exposed copper surface area (S_{Cu}), dispersion of copper (D_{Cu}) and the average Cu particle size (d_{Cu}). The incorporation of Y_2O_3 increased S_{Cu} and D_{Cu} remarkably and a maximum was obtained when Y^{3+}:(Al^{3+}+Y^{3+}) = 0.1, which can be explained by the fact that Y_2O_3 can prevent the aggregation of copper particles during the thermal treatment. However, further increase of Y content declined S_{Cu} and D_{Cu} slightly, which can be attributed to the lower dispersion of ZnO as stated above.

Catalysis Science & Technology Accepted Manuscript

3.3. XPS investigations on reduced samples

XPS analysis was performed to determine the surface chemical states and compositions of reduced CHT-Y*x* catalysts. XPS spectra of the reduced samples are presented in Fig. 5 and Fig. S9. As shown in Fig. 5a, all the spectra consisted of two peaks at 932.5 and 952.5 eV which were mainly attributed to Cu $2p_{3/2}$ and Cu$2p_{1/2}$ peaks of Cu^0, respectively.[12] The absence of satellite peaks around 942 and 962 eV suggested that the Cu^{2+} species were reduced completely after reduction at 573 K. In addition, the line position in the Cu LMM Auger electron spectroscopy of the representative CHT-Y0.1 catalyst also demonstrated that Cu^0 was the predominant copper species detectable on the surface of the reduced catalyst (Fig. 5c). These results are in line with the XRD analysis. After reaction for methanol synthesis from CO_2 hydrogenation, the spent sample presented a principal peak at around 918.4 eV and a smaller peak centered around 916.4 eV (Fig. 5c), which can be attributed to Cu^0 and Cu^+ species within the error limit, respectively, suggesting that some surface Cu^0 species was oxidized to Cu^+ species. However, the identification of Cu^+ species with *ex situ* measurements is not always unambiguous proof that it was present on the surface of the catalyst under reaction condition, because it was hard to totally prevent the sample from exposure to air during separating the used catalyst from the quartz sand. Similar results have been reported for various Cu/ZnO-based catalysts.[12, 45] Consequently, Cu^0 is the predominant copper species on the surface of reduced CHT-Y*x* catalysts according to XRD, XPS and Auger results, which reveals that Cu^+ species cannot be responsible for the activity of these catalysts. Moreover, the Zn $2p_{3/2}$ peak at around 1022.3 eV can be assigned to the Zn^{2+} species on the catalyst surface.

The binding energies (BE) of Cu $2p_{3/2}$, Zn $2p_{3/2}$ and Al 2p bands and surface compositions of the reduced CHT-Y*x* catalysts are listed in Table 3. When Y^{3+}:(Al^{3+}+Y^{3+}) ≤ 0.1, there was no obvious difference in the BE of Cu $2p_{3/2}$ and Zn $2p_{3/2}$ bands with increasing Y content. However, these bands shifted significantly to lower binding energies with further increased Y content, especially for CHT-Y0.5 (Fig. 5b). In addition, the Al 2p core-level was located at BE around 74.7 eV for all the

Catalysis Science & Technology Accepted Manuscript

reduced samples and the BE of Y $3d_{3/2}$ and Y $3d_{5/2}$ changed slightly with increase of Y content (Fig. S9). These results illustrated that there existed interaction among Cu and ZnO and this interaction was weakened with higher Y content, which can be ascribed to lower dispersion of ZnO compared to the samples with Y^{3+}:(Al^{3+}+Y^{3+}) ≤ 0.1. In addition, compared with the bulk compositions taken from Table 1, the surface content of Cu was reduced, while Zn was enriched. The modifier Y accumulated remarkably on the surface for CHT-Y0.05 and CHT-Y0.1 samples, while the surface of reduced catalysts with Y^{3+}:(Al^{3+}+Y^{3+}) > 0.1 was depleted of Y, especially for CHT-Y0.5, which might be related to the significant decrease of the yields of HTl phases in precursors. It can be also found that the surface Cu content and the surface Cu/Zn ratio first increased sharply and then decreased slightly with increasing Y concentration. In a word, the addition of suitable amounts of Y_2O_3 can drastically modify the surface copper/zinc compositions.

3.4. The reducibility of CHT-Y*x* catalysts

The reduction behaviour of the calcined CHT-Y*x* samples was investigated by H_2–TPR, and the corresponding reduction profiles are given in Fig. 6. All samples display a broad reduction peak accompanied by shoulders in the temperature range of 423–623 K, which can be deconvoluted into several Gaussian peaks. The quantitative TPR results including onset reduction temperature ($T_{o,\ red}$), temperature of peak maxima and their contributions are summarized in Table 4.

The low temperature peak (peak β) is attributed to the reduction in dispersed CuO, whereas the peak appearing at high temperature (peak γ) is ascribed to the reduction in bulk CuO. Another peak at even lower temperature (peak α) is observed only on the Y_2O_3-modified sample with Y^{3+}:(Al^{3+}+Y^{3+}) = 0.1, which can be due to the reduction in highly dispersed CuO.[23] Obviously, $T_{o,\ red}$ declined with the introduction of Y_2O_3 and the lowest $T_{o,\ red}$ was obtained over CHT-Y0.1 and further increase of Y content resulted in a increase of $T_{o,\ red}$, in agreement with the *in situ* XRD result. Similar change of the positions of the peaks β and γ could also be observed. These results revealed that suitable amount of Y_2O_3 could enhance the reactivity of the surface Cu^{2+}

Catalysis Science & Technology Accepted Manuscript

species. Furthermore, the contributions of the peaks α and β to the TPR pattern, which represent the amount of easily reducible well-dispersed copper oxide, increased significantly with increase of Y^{3+}:(Al^{3+}+Y^{3+}) atomic ratio, and a maximum of 88.9% was found for the sample with Y^{3+}:(Al^{3+}+Y^{3+}) = 0.1. A slight decrease was observed when the Y content was further increased. This trend is in line with the variation of D_{Cu} determined by means of N_2O chemisorption.

3.5. H_2-TPD analysis

As shown in Fig. 7, two peaks can be observed on all H_2–TPD curves due to different adsorption states of hydrogen species on the surface of the reduced CHT-Y*x* catalysts. The low temperature peak (peak α) around 415 K is H_2 desorbing from surface adsorbed H atoms on surface Cu sites, while a much broader signal (peak β) in the range 573–773 K is attributed to the desorption of strongly adsorbed hydrogen either on the bulk of Cu particles or on the ZnO surface, respectively.[21, 23, 46, 47] Especially, the latter would arise from the "p-type" semiconductor behavior of ZnO induced by the heterolytic split ($H^{\delta+}$–$H^{\delta-}$) of H_2, and the spillover phenomena driven by the "Cu–ZnO" interaction significantly influenced the H_2 adsorption on ZnO.[46-48]

The maximum desorption temperature and quantitative data are listed in Table 5. The position of peak α changed slightly with increased Y content, while the maximum desorption temperature of peak β increased when the Y^{3+}:(Al^{3+}+Y^{3+}) atomic ratio was above 0.1. This phenomenon also suggested a relatively weaker interaction between Cu and ZnO, which agreed with the XPS and HRTEM results. In addition, the H_2 desorption amount evolving from Cu sites increased sharply and the maximum of H_2 adsorption was obtained over CHT-Y0.1, while it decreased slightly with further increase of Y content, which is in accordance with the variation of S_{Cu}. From the data of peak β, the H_2 desorption amount at high temperature decreased gradually with increased Y content. This trend was significant when Y^{3+}:(Al^{3+}+Y^{3+}) ≤ 0.1, which can be ascribed to the remarkable decrease of the amount of bulk Cu particles according to the TPR analysis. When Y^{3+}:(Al^{3+}+Y^{3+}) > 0.1, the amount of bulk Cu particles increased slightly, while the dispersion of ZnO became much lower. Therefore, the

Catalysis Science & Technology Accepted Manuscript

slight decrease of the H_2 desorption amount of peak β with further increase of Y content is easy to understand by considering these two factors.

3.6. Catalytic behaviour

As well known, there are two important competitive reactions in CO_2 hydrogenation to methanol. The first one is the synthesis of methanol (3) and the second one is the reverse water gas shift (RWGS) reaction (4). The equilibrium of such reactions can be described as follows:

$$CO_2 + 3H_2 \rightleftharpoons CH_3OH + H_2O \qquad \Delta H_{298K,\ 5MPa} = -40.9\ kJ\ mol^{-1} \qquad (3)$$

$$CO_2 + H_2 \rightleftharpoons CO + H_2O \qquad \Delta H_{298K,\ 5MPa} = 49.8 kJ\ mol^{-1} \qquad (4)$$

Catalytic performance of $Cu/ZnO/Al_2O_3$ catalyst and Y_2O_3-modified $Cu/ZnO/Al_2O_3$ catalysts in methanol synthesis from CO_2 hydrogenation are summarized in Table 6. The major product is CH_3OH and the main byproduct is CO under the operating conditions of T = 503 K, P = 5.0 MPa and GHSV = 10,000 mL $gcat^{-1}$ h^{-1}. In addition, trace of CH_4 is also detected. The Y_2O_3-modified $Cu/ZnO/Al_2O_3$ catalysts exhibited much better catalytic performance compared to $Cu/ZnO/Al_2O_3$ catalyst, and the conversion of CO_2 and the yield of CH_3OH increased by 13–51% and 16–56%, respectively. In addition, both the CO_2 conversion and the CH_3OH yield took on a volcanic trend with increase of Y content. A maximum CH_3OH yield of 0.39 g $gcat^{-1}$ h^{-1} with the CO_2 conversion of 20.2% and the CH_3OH selectivity of 69.3% is obtained over the $Cu/ZnO/Al_2O_3/Y_2O_3$ catalyst with Y^{3+}:(Al^{3+}+Y^{3+}) = 0.1 at 503 K.

The effects of reaction pressure on the catalytic performance of CHT-Y*x* catalysts (*x* = 0, 0.1, 0.5) are shown in Fig. 8. It can be seen that both the conversion of CO_2 and selectivity of methanol increased significantly with increase of reaction pressure. For CHT-Y0.1 sample, the CO_2 conversion increased from 9.9% to 29.9% and the methanol selectivity increased from 15.1% to 89.7% when the total pressure was raised from 0.3 MPa to 9.0 MPa. This tendency can be explained by Le Chatelier's principle as the methanol synthesis reaction (3) proceeds under a volume contraction. In addition, the rate of reaction increases kinetically with the increase in pressure.

Catalysis Science & Technology Accepted Manuscript

Therefore, higher CO_2 conversion and CH_3OH selectivity were obtained at higher pressures. In addition, in the whole pressure range, both the CO_2 conversion and CH_3OH selectivity for CHT-Y0.1 were higher than those for CHT-Y0 and CHT-Y0.5 samples. The variation in CH_3OH yield versus pressure is similar to those in CO_2 conversion and CH_3OH selectivity (Fig. S10). At a pressure of 9.0 MPa, the yield of methanol reached 0.57 g $gcat^{-1}$ h^{-1} for CHT-Y0.1.

3.7. Correlations between activity and structural parameters

The turnover frequency (TOF), which represents the number of CO_2-molecule hydrogenated on unit site of exposed copper atom per second (s^{-1}), was calculated from the exposed copper surface area for various catalysts. Results from this study (see Table 6) showed that the TOF decreased continuously with increase of Y content and a minimum TOF of 5.53×10^{-3} was obtained over CHT-Y0.5 at 503 K. This change was not consistent with the trend of the Cu crystallite size and similar results were reported by other researchers.[16, 21] Therefore, methanol synthesis from CO_2 hydrogenation is structurally sensitive.

To gain further insight into the nature of active species in methanol synthesis from CO_2 hydrogenation, we attempted to correlate CO_2 conversion with the exposed copper surface area determined by N_2O chemisorption. Variations of the CO_2 conversion and the exposed copper surface area as a function of Y^{3+}:(Al^{3+}+Y^{3+}) atomic ratio for CHT-Y*x* catalysts are displayed in Fig. 9. Notably, when Y^{3+}:(Al^{3+}+Y^{3+}) ≤ 0.1, the variation of CO_2 conversion was consistent with the trend of the S_{Cu}, giving clear evidence that metallic Cu involved as the active site in CO_2 hydrogenation to methanol. The metallic copper surface was mainly responsible for the catalytic activity, which can offer a rational explanation for the promoting effect of yttrium oxide on the catalytic performance. When Y^{3+}:(Al^{3+}+Y^{3+}) > 0.1, there existed some difference between the variation of CO_2 conversion and S_{Cu}. S_{Cu} declined slightly with further increase of Y content, while the conversion of CO_2 decreased significantly, which revealed that catalytic activity in CO_2 hydrogenation to methanol not only depended on the metallic copper surface but also other factors. It is a popular viewpoint that two active sites are involved in the methanol synthesis from CO_2

Catalysis Science & Technology Accepted Manuscript

hydrogenation over the Cu/ZnO-based catalysts.[23, 16, 46, 48] The adsorption and dissociation of hydrogen occur on the Cu sites, while the adsorption of CO_2 takes place over the ZnO sites. The atomic hydrogen transports from the surface of Cu onto the surface of ZnO sites via spillover and hydrogenates the adsorbed carbon-containing species to form methanol. Therefore, many authors believed that metal/oxides interface played an important role in CO_2 hydrogenation to methanol.[22, 46, 49] In our case, the interaction between Cu and ZnO is weakened with further increase of Y content as a result of the significant decrease of amounts of HTl phases in precursors from XPS, HRTEM and H_2–TPD analysis, which can decrease the catalytic activity. Obviously, an efficient interaction among the metallic Cu and the ZnO sites is also necessary to ensure high catalytic activity in methanol synthesis from CO_2 hydrogenation.

3.8. Stability of catalysts

Long-term stability of catalysts is vital for methanol synthesis from CO_2 hydrogenation. Under the conditions of T = 523 K, P = 5.0 MPa and GHSV = 10,000 mL $gcat^{-1}$ h^{-1}, comparisons of CO_2 conversion and CH_3OH yield as a function of reaction time for CHT-Y0, CHT-Y0.1 and CHT-Y0.5 catalysts are shown in Fig. 10. After 500 h reaction over the CHT-Y0 catalyst, the conversion of CO_2 and the yield of CH_3OH were found to decrease by 10.0% and 8.3% from its initially stabilized values, respectively. With the incorporation of Y_2O_3, the stability of the Cu/ZnO/Al_2O_3 catalyst was enhanced markedly. As shown in Fig. 10, no obvious decline in the activity was observed after 500 h time-on-stream over CHT-Y0.1. The CO_2 conversion and CH_3OH yield only decreased by 3.4% and 4.3%, respectively. However, with the introduction of excess Y content, the catalytic activity of CHT-Y0.5 was less stable than that of CHT-Y0.1, and the conversion of CO_2 and the yield of CH_3OH were found to decrease by 5.4% and 6.2%, respectively.

The XRD data in Fig. 11 suggested that the Cu particle size of spent CHT-Y0 catalyst after 500 h grew significantly from 13.7 to 17.6 nm due to remarkable agglomeration of copper species. In contrast, the size of crystal of Cu increased

Catalysis Science & Technology Accepted Manuscript

moderately with the introduction of Y_2O_3. The Cu particle size of spent CHT-Y0.1 increased by 13.3 % (8.3→9.4 nm) from the value of CHT-Y0.1 after *ex situ* reduction. For the spent CHT-Y0.5 catalyst, the Cu particle size increased by 18.3 % (9.3→11.0 nm) which was higher than that of spent CHT-Y0.1. Similar results have been obtained from above analysis of the *in situ* XRD measurement.

3.9. Discussion on the effects of Y content on the CO_2 hydrogenation

With the introduction of Y_2O_3 into $Cu/ZnO/Al_2O_3$ catalysts, the catalytic performance for CO_2 hydrogenation to methanol was improved markedly due to the significant increase of S_{Cu} and D_{Cu}. However, when $Y^{3+}:(Al^{3+}+Y^{3+}) > 0.1$, the dispersion of Cu would decrease slightly and the interaction between Cu and ZnO was weakened due to the lower dispersion of ZnO as a result of the declined amount of HTl phases in the precursor. Therefore, the catalytic activity decreased when $Y^{3+}:(Al^{3+}+Y^{3+}) > 0.1$ and the $Cu/ZnO/Al_2O_3/Y_2O_3$ catalyst with $Y^{3+}:(Al^{3+}+Y^{3+}) = 0.1$ showed the highest activity for the methanol synthesis reaction.

During CO_2 hydrogenation, equimolar amount of water is inevitably produced from the main reactions (3)–(4). Some researchers asserted that the low stability of the $Cu/ZnO/Al_2O_3$ catalyst was partly attributed to sintering of Cu nanoparticles accelerated by water, which can result in a tremendous loss of copper surface area [12, 14, 50]. In our case, the stability of the $Cu/ZnO/Al_2O_3$ catalyst was improved significantly with the incorporation of Y_2O_3, because Y_2O_3 could prevent the aggregation of Cu nanoparticles during the process of reaction, which was well interpreted by the results of XRD. However, the stability of the $Cu/ZnO/Al_2O_3$ catalyst became lower with the introduction of excess Y_2O_3. As stated above, the HTl structure could immobilize copper species and suppress sintering of copper particles during thermal treatment. Thus, the lower stability for CHT-Y0.5 could be attributed to the decreased amount of HTl phases in the precursor compared to CHT-Y0.1. In addition, the formation of water should be responsible for a partial oxidation of the metallic sites (CuO_x), which can decrease the activity of methanol synthesis catalyst.[14, 22] The oxidized CuO_x can be reduced by H_2 or CO and the effect of CuO_x on catalytic

Catalysis Science & Technology Accepted Manuscript

activity will become smaller when the reduction reaction rate is high. According to TPR and *in situ* XRD results, the addition of Y_2O_3 could improve the catalyst reducibility remarkably, while the introduction of excess Y_2O_3 weakened copper reducibility due to the declined amount of HTl phases in the precursor, which indicated that the rate of reduction in CuO_x for CHT-Y0.1 was higher than those for CHT-Y0 and CHT-Y0.5. This could also interpret the higher catalytic stability for CO_2 hydrogenation to methanol. Therefore, the incorporation of Y_2O_3 and the HTl structure can improve stability of the $Cu/ZnO/Al_2O_3$ catalyst.

4. Conclusion

It has been concluded that the introduction of Y_2O_3 into $Cu/ZnO/Al_2O_3$ catalysts derived from hydrotalcite-like precursors increased the surface area and dispersion of Cu. However, the ZnO dispersion in reduced catalysts became lower with the introduction of excess Y content attributed to the declined amount of hydrotalcite-like phases in precursors, which would decrease the dispersion of Cu slightly and weaken the interaction between Cu and ZnO. In addition, Y_2O_3 and the hydrotalcite-like structure could prevent the aggregation of Cu nanoparticles during heat treatment and reaction and improve the reducibility of Cu^{2+} species.

XRD, XPS and Auger characterizations demonstrated that Cu^0 species were predominant active sites for the methanol synthesis from CO_2 hydrogenation. Addition of suitable amount of Y_2O_3 to $Cu/ZnO/Al_2O_3$ catalyst remarkably enhanced the catalytic performance for CO_2 hydrogenation. When $Y^{3+}:(Al^{3+}+Y^{3+}) > 0.1$, the conversion of CO_2 decreased significantly due to the lower Cu surface area and a relatively weaker interaction between Cu and ZnO. A maximum CH_3OH yield of 0.57 g $gcat^{-1}$ h^{-1} with the CO_2 conversion of 29.9% and the CH_3OH selectivity of 89.7% was obtained over the $Cu/ZnO/Al_2O_3/Y_2O_3$ catalyst with $Y^{3+}:(Al^{3+}+Y^{3+}) = 0.1$ at 503 K and 9.0 MPa.

The decrease of catalytic activity during the long-term test was mainly related to the agglomeration of Cu nanoparticles and partial oxidation of Cu^0 species. The activity of $Cu/ZnO/Al_2O_3/Y_2O_3$ catalyst with $Y^{3+}:(Al^{3+}+Y^{3+}) = 0.1$ was more stable

Catalysis Science & Technology Accepted Manuscript

than those of $Cu/ZnO/Al_2O_3$ and $Cu/ZnO/Al_2O_3/Y_2O_3$ with $Y^{3+}:(Al^{3+}+Y^{3+}) = 0.5$ catalysts, indicating the incorporation of Y_2O_3 and the hydrotalcite-like structure can improve stability of the $Cu/ZnO/Al_2O_3$ catalyst.

Acknowledgements

This work was financially supported by the National Key Technology Research and Development Program of the Ministry of Science and Technology of China (2013BAC11B02), Strategic Priority Research Program of the Chinese Academy of Sciences (XDA02040602) and Shanghai Municipal Science and Technology Commission, China (15ZR1444500).

Catalysis Science & Technology Accepted Manuscript

Reference

1 X. W. Zhou, J. Qu, F. Xu, J. P. Hu, J. S. Foord, Z. Y. Zeng, X. L. Hong, S. C. E. Tsang, *Chem. Commun.*, 2013, **49**, 1747-1749.

2 M. Aresta, A. Dibenedetto, A. Angelini, *J. CO2 Util.*, 2013, **3-4**, 65-73.

3 G.A. Olah, A. Geoppert, G.K.S. Prakash, Beyond Oil and Gas: The Methanol Economy, first ed., Wiley-VCH, Weinheim, 2006. pp. 173–187, 239–245.

4 J. Choudhury, *ChemCatChem*, 2012, **4**, 609-611.

5 G.A. Olah, G.K.S. Prakash, A. Goeppert, *J. Am. Chem. Soc.*, 2011, **133**, 12881-12898.

6 A. Bansode, B. Tidona, P. R. von Rohr, A. Urakawa, *Catal. Sci. Technol.*, 2013, **3**, 767-778.

7 Z.S. Hong, Y. Cao, J.F. Deng, K.N. Fan, *Appl. Catal., A*, 2002, **82**, 37-44.

8 F. Pontzen, W. Liebner, V. Gronemann, M. Rothaemel, B. Ahlers, *Catal. Today*, 2011, 171, 242-250.

9 P. Gao, F. Li, L. Zhang, N. Zhao, F. Xiao, W. Wei, L. Zhong, Y. Sun, *J. CO2 Util.*, 2013, **2**, 16-23.

10 Q. Sun, Y.L. Zhang, H.Y. Chen, J.F. Deng, D. Wu, S.Y. Chen, *J. Catal.*, 1997, 167, 92-105.

11 A. Bansode, A. Urakawa, *J. Catal.*, 2014, **309**, 66-70.

12 S. Natesakhawat, J.W. Lekse, J.P. Baltrus, P.R. Ohodnicki, B.H. Howard, X.Y. Deng, C. Matranga, *ACS Catal.*, 2012, **2**, 1667-1676.

13 X.M. Guo, D.S. Mao, G.Z. Lu, S. Wang, G.S. Wu, *J. Catal.*, 2010, **271**, 178-185.

14 C. Li, X. Yuan, K. Fujimoto, *Appl. Catal., A*, 2014, **469**, 306-311.

15 P. Gao, F. Li, N. Zhao, H. Wang, W. Wei, Y. H. Sun, *Acta Phys.-Chim. Sin.,* 2014, 30, 1155-1162.

16 X. Guo, D. Mao, G. Lu, S. Wang, G. Wu, *J. Mol. Catal. A: Chem.*, 2011, **345**, 60-68.

17 H. Jeong, C.H. Cho, T.H. Kim, *React. Kinet. Mech. Cat.*, 2012, **106**, 435-443.

18 P. Gao, F. Li, N. Zhao, F.K. Xiao, W. Wei, L.S. Zhong, Y.H. Sun, *Appl. Catal., A*, 2013, **468**, 442-452.

19 T. Witoon, T. Permsirivanich, W. Donphai, A. Jaree, M. Chareonpanich, *Fuel Process. Technol.*, 2013, **116**, 72-78.

20 P. Gao, F. Li, H.J. Zhan, N. Zhao, F.K. Xiao, W. Wei, L.S. Zhong, Y.H. Sun, *Catal. Commun.*, 2014, **50**, 78-82.

21 F. Arena, K. Barbera, G. Italiano, G. Bonura, L. Spadaro, F. Frusteri, *J. Catal.*, 2007, **249**, 185-194.

22 G. Bonura, M. Cordaro, C. Cannilla, F. Arena, F. Frusteri, *Appl. Catal., B*, 2014, **152**, 152-161.

23 P. Gao, F. Li, H.J. Zhan, N. Zhao, F.K. Xiao, W. Wei, L.S. Zhong, H. Wang, Y.H. Sun, *J. Catal.*, 2013, **298**, 51-60.

24 M. Behrens, F. Studt, I. Kasatkin, S. Kuhl, M. Havecker, F. Abild-Pedersen, S. Zander, F. Girgsdies, P. Kurr, B.L. Kniep, M. Tovar, R.W. Fischer, J.K. Norskov, R. Schlogl, *Science*, 2012, **336**, 893-897.

25 R. Ladera, F.J. Perez-Alonso, J.M. Gonzalez-Carballo, M. Ojeda, S. Rojas, J.L.G. Fierro, *Appl. Catal., B*, 2013, **142**, 241-248.

26 J. Toyir, P.R. de la Piscina, J.L.G. Fierro, N. Homs, *Appl. Catal., B*, 20012, **9**, 207-215.

27 K.P. Sun, W.W. Lu, F.Y. Qiu, S.W. Liu, X.L. Xu, *Appl. Catal., A*, 2003, **252**, 243-249.

Catalysis Science & Technology Accepted Manuscript

28 C. Baltes, S. Vukojevic, F. Schuth, *J. Catal.*, 2008, **258**, 334-344.

29 K. Nishida, I. Atake, D. Li, T. Shishido, Y. Oumi, T. Sano, K. Takehira, *Appl. Catal., A*, 2008, **337**, 48-57.

30 A. Alejandre, F. Medina, P. Salagre, X. Correig, J.E. Sueiras, *Chem. Mater.*, 1999, **11**, 939-948.

31 G. Busca, U. Costantino, F. Marmottini, T. Montanari, P. Patrono, F. Pinzari, G. Ramis, *Appl. Catal., A*, 2006, **310**, 70-78.

32 L.H. Zhang, C. Zheng, F. Li, D.G. Evans, X. Duan, *J. Mater. Sci.*, 2008, 43, 237-243.

33 P. Gao, F. Li, F.K. Xiao, N. Zhao, N.N. Sun, W. Wei, L.S. Zhong, Y.H. Sun, *Catal. Sci. Technol.*, 2012, **2**, 1447-1454.

34 A. Venugopal, J. Palgunadi, J.K. Deog, O.S. Joo, C.H. Shin, *J. Mol. Catal. A: Chem.*, 2009, **30**, 220-27.

35 P. Clancy, J.P. Breen, J.R.H. Ross, *Catal. Today*, 2007,**127**, 291-294.

36 J. Cheng, X.P. Wang, J.J. Yu, Z.P. Hao, Z.P. Xu, *J. Phys. Chem. C*, 2011, **115**, 6651-6660.

37 J.M. Fernandez, C. Barriga, M.A. Ulibarri, F.M. Labajos, V. Rives, *Chem. Mater.*, 1997, **9**, 312-318.

38 S. Velu, D.P. Sabde, N. Shah, S. Sivasanker, *Chem. Mater.*, 1998, **10**, 3451-3458.

39 E. Frei, A. Schaadt, T. Ludwig, H. Hillebrecht, I. Krossing, *ChemCatChem*, 2014, **6**, 1721-1730.

40 G.D. Wu, X.L. Wang, B. Chen, J.P. Li, N. Zhao, W. Wei, Y.H. Sun, *Appl. Catal., A*, 2007, **329**, 106-111.

41 M. Behrens, I. Kasatkin, S. Kuhl, G. Weinberg, *Chem. Mater.*, 2010, **22**, 386-397.

42 Q. Zhang, Y.Z. Zuo, M.H. Han, J.F. Wang, Y. Jin, F. Wei, *Catal. Today*, 2010, **150**, 55-60.

43 X. An, J.L. Li, Y.Z. Zuo, Q. Zhang, D.Z. Wang, J.F. Wang, *Catal. Lett.*, 2007, **118**, 264-269.

44 M. Behrens, *J. Catal.*, 2009, **267**, 24-29.

45 J. Yoshihara, S.C. Parker, A. Schafer, C.T. Campbell, *Catal. Lett.*, 1995, **31**, 313-324.

46 F. Arena, G. Italiano, K. Barbera, S. Bordiga, G. Bonura, L. Spadaro, F. Frusteri, *Appl. Catal., A*, 2008, **350**, 16-23.

47 H. Wilmer, T. Genger, O. Hinrichsen, *J. Catal.*, 2003, **215**, 188-198.

48 X.M. Liu, G.Q. Lu, Z.F. Yan, J. Beltramini, *Ind. Eng. Chem. Res.*, 2003, **42**, 6518-6530.

49 J. Sloczynski, R. Grabowski, A. Kozlowska, P. Olszewski, J. Stoch, J. Skrzypek, M. Lachowska, *Appl. Catal., A*, 2004, **278**, 11-23.

50 M. Kilo, J. Weigel, A. Wokaun, R.A. Koeppel, A. Stoeckli, A. Baiker, *J. Mol. Catal. A: Chem.*, 1997, **126**, 169-184.

Catalysis Science & Technology Accepted Manuscript

Table 1

Structural parameters and weight loss of the synthesized hydrotalcite-like precursors.

Sample	Y /(Al+Y) Atomic ratio [a]	a (Å)	c (Å)	Weight Loss (%)			
				Total	first	second	third
HT-Y0	0	3.078	22.73	28.5	12.0	11.0	5.5
HT-Y0.05	0.05	3.080	22.76	31.0	10.5	15.0	5.5
HT-Y0.1	0.1	3.082	22.93	31.0	10.5	16.0	4.5
HT-Y0.2	0.2	3.083	23.09	31.0	11.0	16.0	4.0
HT-Y0.5	0.5	-	23.09	31.0	12.0	15.5	3.5

Catalysis Science & Technology Accepted Manuscript

Table 2

Physicochemical properties of the calcined CHT-Y*x* samples.

Sample	Metal composition (mol%) [a]				Cu:Zn [a]	Y:(Al+Y) [a]	S_{BET}	V_p	d_{Cu} [b]	S_{Cu} [c]	D_{Cu} [c]	d_{Cu} [c]
	Cu	Zn	Al	Y			($m^2 g^{-1}$)	($cm^3 g^{-1}$)	(nm)	($m^2 g^{-1}$)	(%)	(nm)
CHT-Y0	51.0	24.8	24.2	-	2.06	-	39	0.20	13.7	17.4	6.72	13.4
CHT-Y0.05	51.6	23.6	23.3	1.5	2.18	0.06	74	0.44	11.0	30.8	10.87	9.6
CHT-Y0.1	51.1	23.5	22.4	3.0	2.17	0.12	108	0.61	8.3	34.3	13.60	7.6
CHT-Y0.2	51.0	23.9	19.3	5.8	2.14	0.23	108	0.76	8.8	33.8	13.17	7.9
CHT-Y0.5	50.0	23.6	11.9	14.5	2.12	0.55	98	0.77	9.3	33.4	12.83	8.1

[a] Values measured by ICP; [b] Average Cu particle size calculated by XRD; [c] Calculated from N_2O dissociative adsorption.

Catalysis Science & Technology Accepted Manuscript

Table 3

XPS results for the reduced $Cu/ZnO/Al_2O_3$ catalysts with different Y content.

Sample	Binding energy (eV)			Relative surface concentration of metal (at.%)				Cu/Zn
	Cu $2p_{3/2}$	Zn $2p_{3/2}$	Al 2p	Cu	Zn	Al	Y	
CHT-Y0	932.6	1022.3	74.6	34.2	32.2	33.6	0	1.06
CHT-Y0.05	932.7	1022.4	74.8	39.7	30.4	26.9	3.0	1.31
CHT-Y0.1	932.6	1022.3	74.6	41.9	29.7	23.7	4.7	1.41
CHT-Y0.2	932.3	1021.9	74.6	40.3	29.2	25.3	5.2	1.38
CHT-Y0.5	932.2	1021.7	74.8	39.3	28.6	22.9	9.2	1.37

Catalysis Science & Technology Accepted Manuscript

Table 4

Onset temperature of reduction ($T_{o,\ red}$), temperature of peak maxima and contribution of each peak to the TPR pattern.

Sample	$T_{o,\ red}$ (K)	Temperature of peak maxima (K) and concentration (%) [a]		
		Peak α	Peak β	Peak γ
CHT-Y0	460	-	536 (48.5)	591(51.5)
CHT-Y0.05	438	-	540 (76.2)	575 (23.8)
CHT-Y0.1	430	510 (37.1)	530 (51.8)	545 (11.1)
CHT-Y0.2	440	-	517 (85.9)	547 (14.1)
CHT-Y0.5	442	-	513 (85.2)	543 (14.8)

[a] Values in parentheses are the contribution (%) of each species.

Catalysis Science & Technology Accepted Manuscript

Table 5

The maximum temperature and amount of H_2 desorption over reduced CHT-Y*x* catalysts.

Sample	Peak α		Peak β	
	T (K)	H_2 desorption (μmol g^{-1})	T (K)	H_2 desorption (μmol g^{-1})
CHT-Y0	406	20.4	657	392.8
CHT-Y0.05	412	64.0	657	206.0
CHT-Y0.1	419	115.0	659	114.3
CHT-Y0.2	415	111.9	665	102.5
CHT-Y0.5	415	108.5	676	97.6

Catalysis Science & Technology Accepted Manuscript

Table 6

The catalytic performance for methanol synthesis from CO_2 hydrogenation over CHT-Y*x* catalysts derived from hydrotalcite-like precursors.

Sample	CO_2 Conversion (%)	TOF×10^3 (s^{-1})	Selectivity (C-mol%)			CH_3OH Yield (g $gcat^{-1}$ h^{-1})
			CH_3OH	CH_4	CO	
CHT-Y0	13.4	8.33	58.1	0.3	41.6	0.25
CHT-Y0.05	17.4	6.95	63.2	0.2	36.6	0.33
CHT-Y0.1	20.2	6.66	69.3	0.2	30.5	0.39
CHT-Y0.2	17.8	6.22	70.5	0.1	29.4	0.35
CHT-Y0.5	15.1	5.53	66.6	0.3	33.1	0.29

Reaction conditions: T = 503 K, P = 5.0 MPa, GHSV = 10,000 mL $gcat^{-1}$ h^{-1}, $H_2/CO_2/N_2$= 73/24/3 (molar ratio).

Catalysis Science & Technology Accepted Manuscript

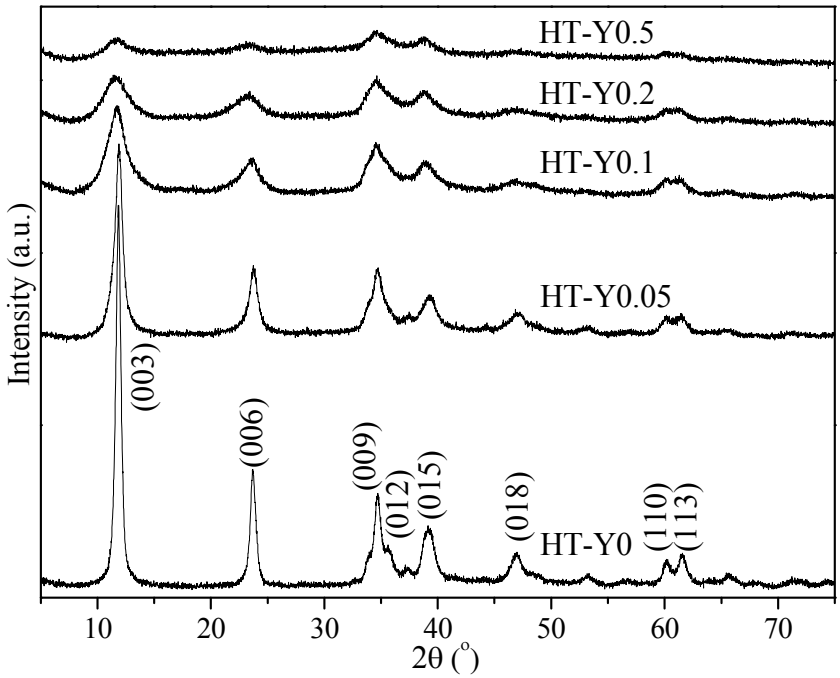

Fig. 1. XRD patterns of the uncalcined HT-Y*x* precursors.

Catalysis Science & Technology Accepted Manuscript

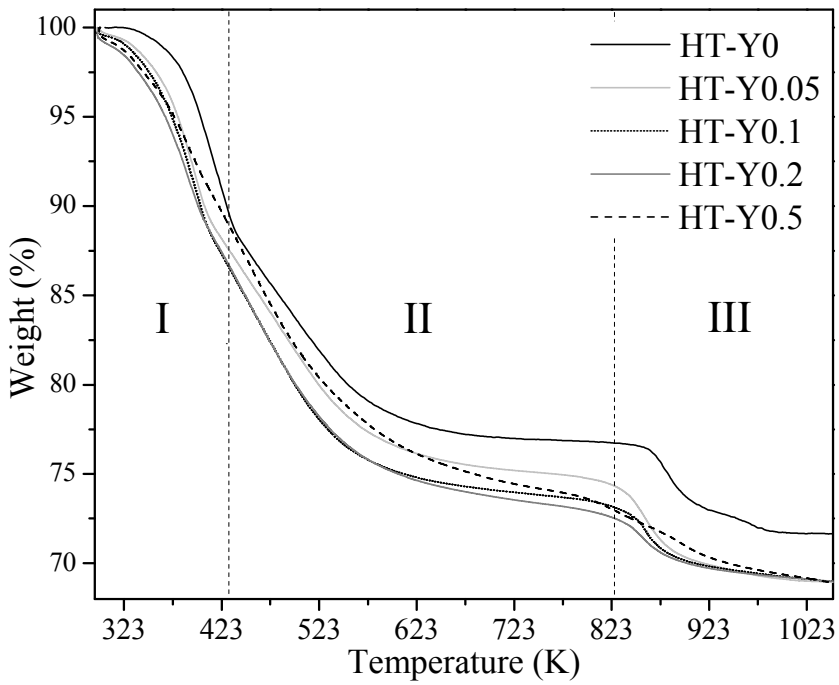

Fig. 2. Thermogravimetry and differential thermogravimetry (TG-DTG) profiles of HT-Y*x* precursors in air.

Catalysis Science & Technology Accepted Manuscript

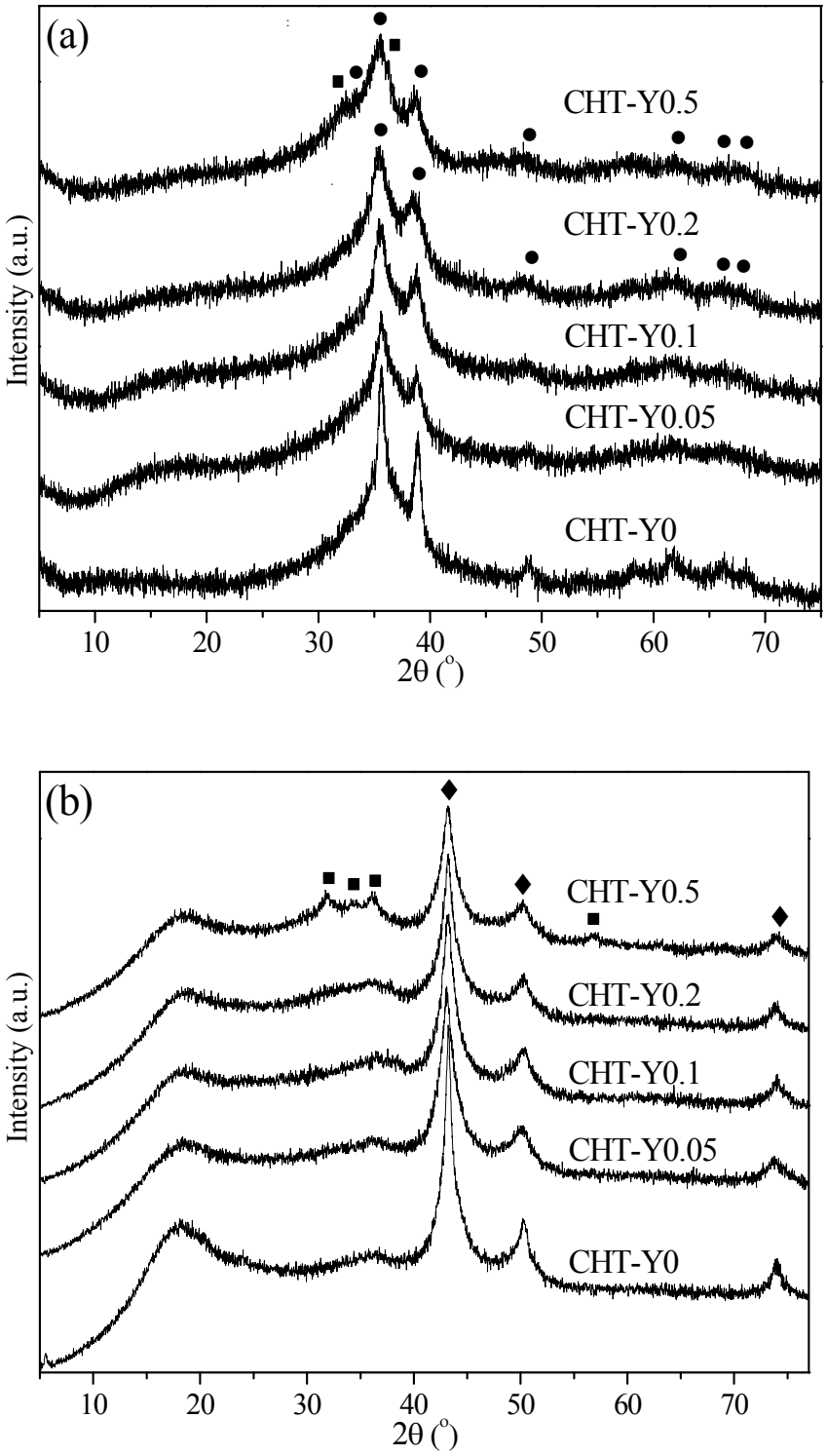

Fig. 3. XRD patterns of $Cu/ZnO/Al_2O_3$ catalysts with different Y content upon (a) calcination; (b) reduction. (●) CuO; (◆)Cu; (■) ZnO.

Catalysis Science & Technology Accepted Manuscript

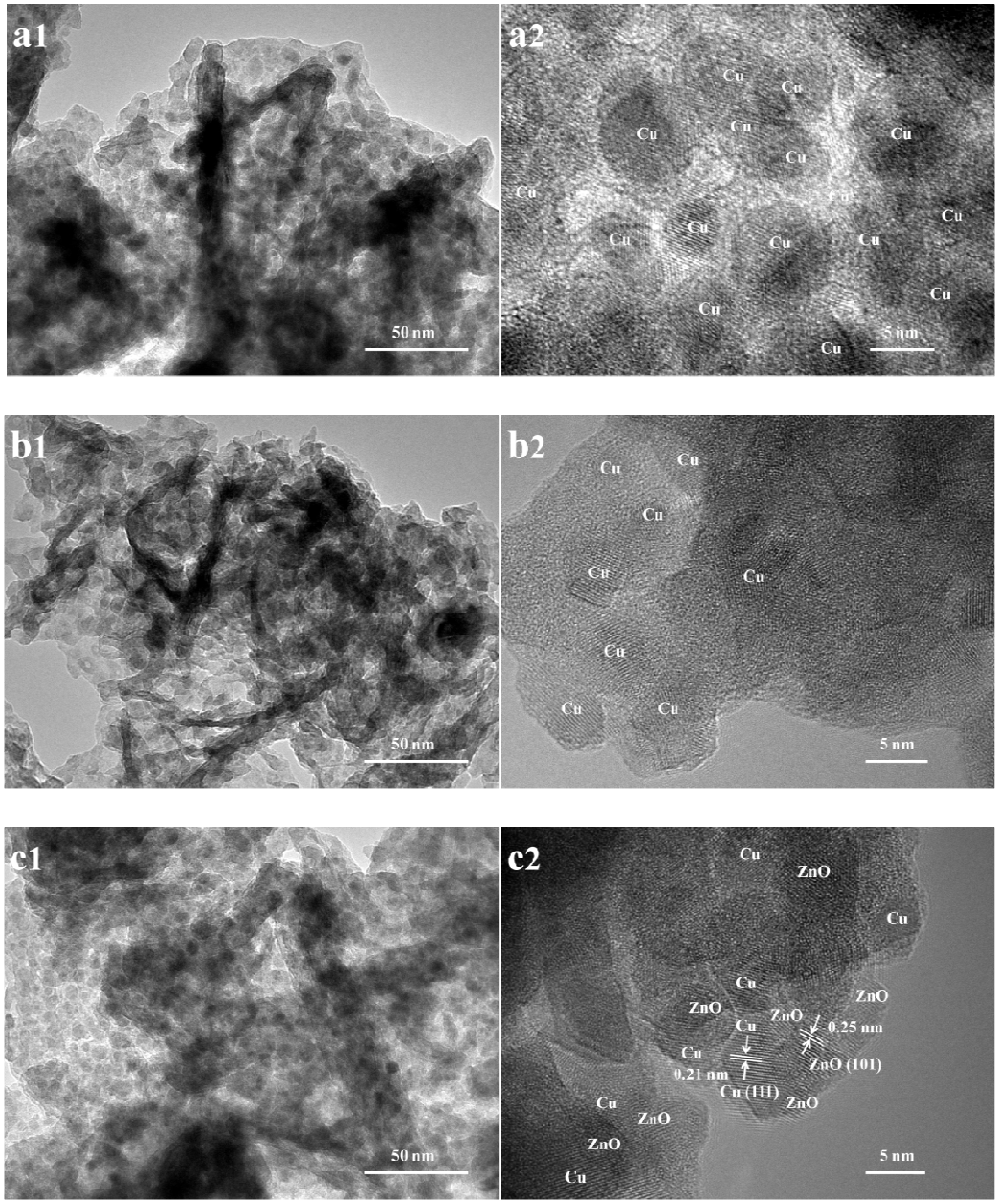

Fig. 4. TEM and HRTEM images of CHT-Y*x* samples after reduction at 573 K for 6 h: (a) CHT-Y0, (b) CHT-Y0.1, (c) CHT-Y0.5.

Catalysis Science & Technology Accepted Manuscript

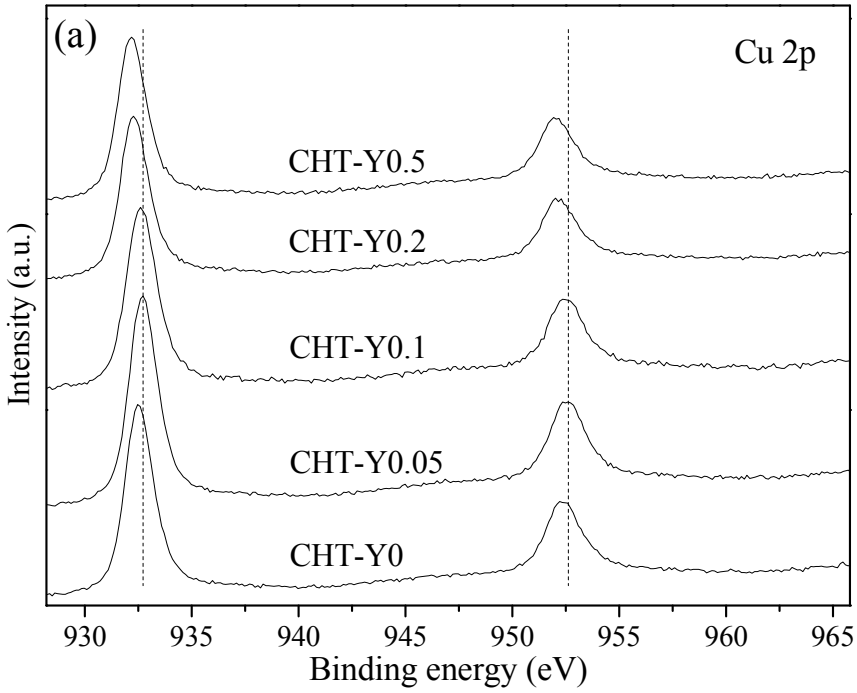

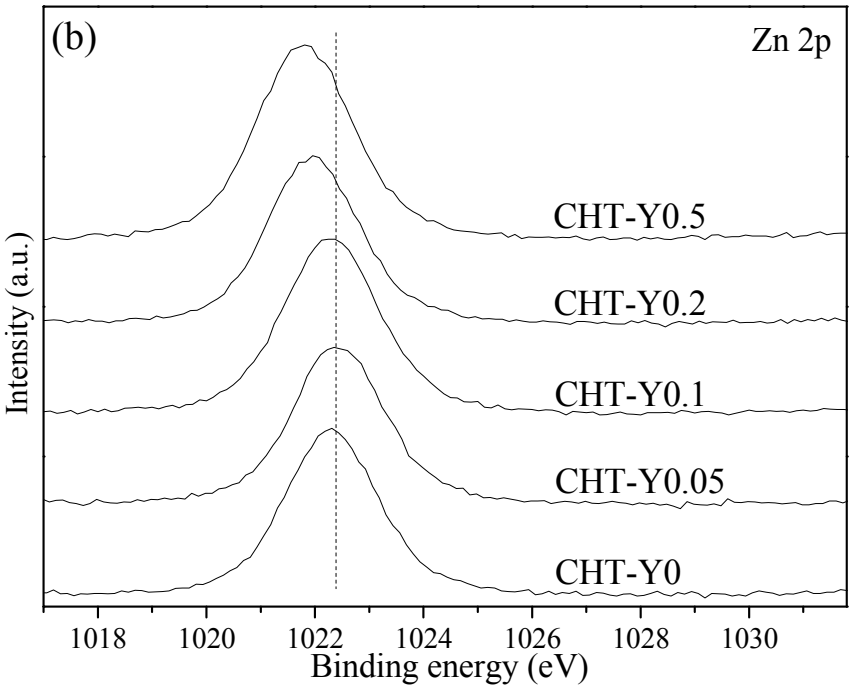

Catalysis Science & Technology Accepted Manuscript

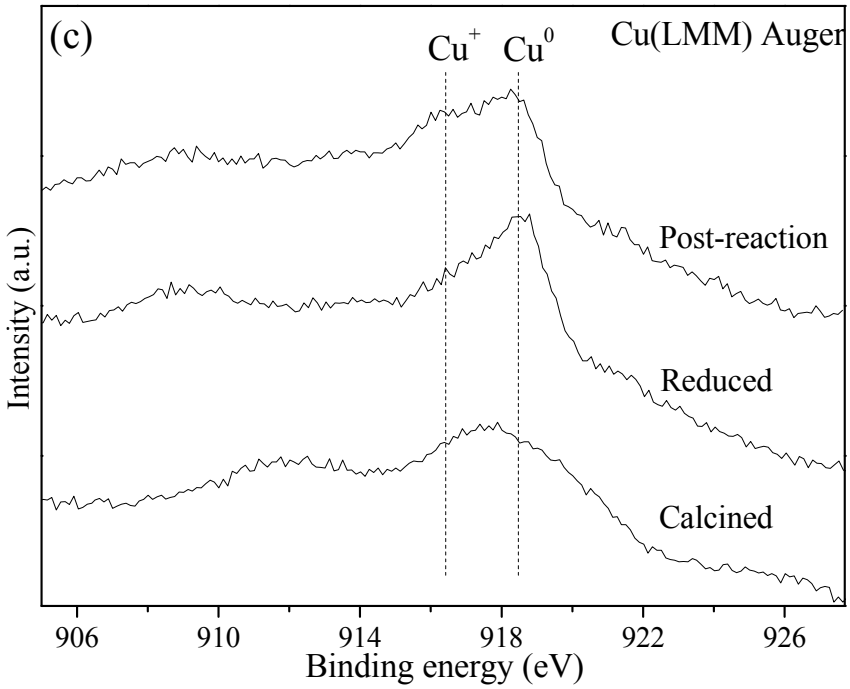

Fig. 5. (a) Cu 2p and (b) Zn 2p XPS of the reduced CHT-Y*x* catalysts, and (c) Cu LMM Auger spectra for the CHT-Y0.1 catalyst after different treatments.

Catalysis Science & Technology Accepted Manuscript

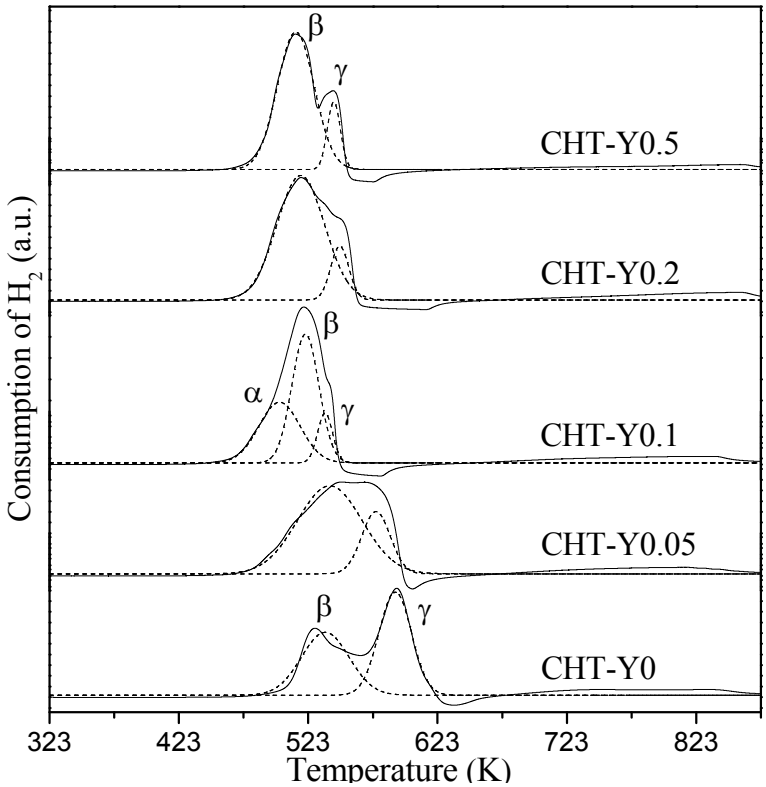

Fig. 6. TPR profiles of the $Cu/ZnO/Al_2O_3$ catalysts with different Y content.

Catalysis Science & Technology Accepted Manuscript

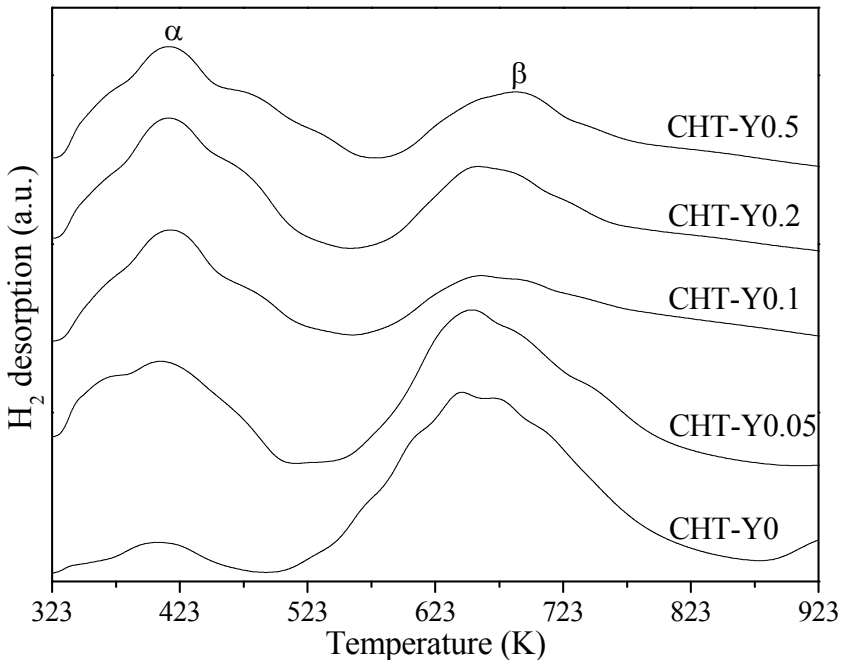

Fig. 7. H_2-TPD profiles of the reduced CHT-Y*x* catalysts.

Catalysis Science & Technology Accepted Manuscript

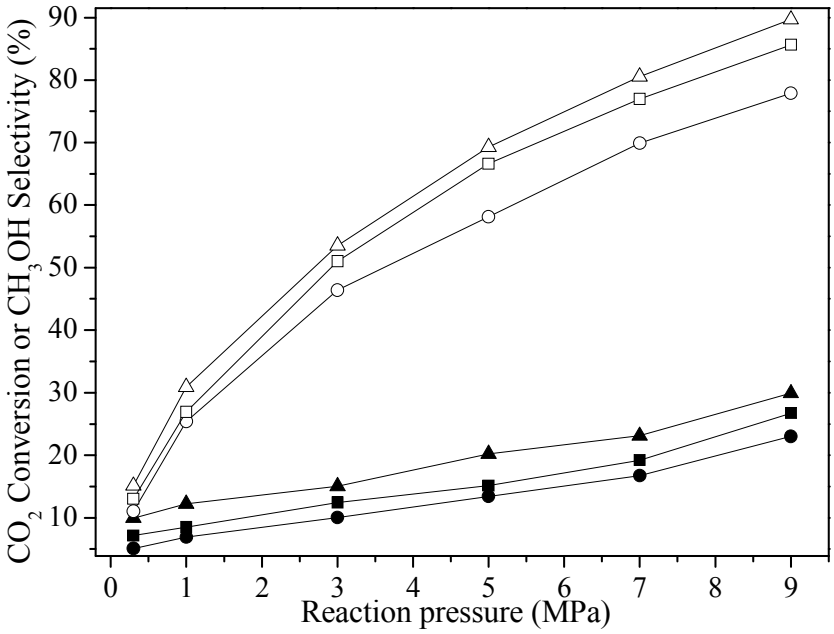

Fig. 8. Effect of reaction pressure on the conversion of CO_2 (solid symbols) and selectivity of methanol (open symbols) over CHT-Y*x* catalysts: (circles) CHT-Y0; (triangles) CHT-Y0.1; (rectangles) CHT-Y0.5. Reaction conditions: T = 503 K, GHSV = 10,000 mL $gcat^{-1}$ h^{-1}, $H_2/CO_2/N_2$ = 73/24/3 (molar ratio).

Catalysis Science & Technology Accepted Manuscript

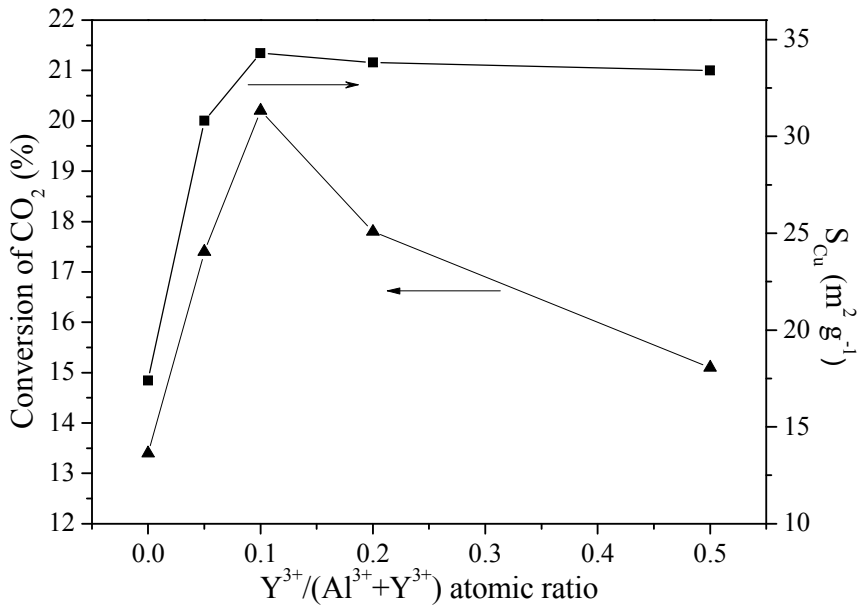

Fig. 9. Variations of the CO_2 conversion and the exposed copper surface area as a function of Y^{3+}:(Al^{3+}+Y^{3+}) atomic ratio for CHT-Y*x* catalysts. Reaction conditions: T=503 K, P = 5.0 MPa, GHSV = 10,000 mL $gcat^{-1}$ h^{-1}, $H_2/CO_2/N_2$= 73/24/3 (molar ratio).

Catalysis Science & Technology Accepted Manuscript

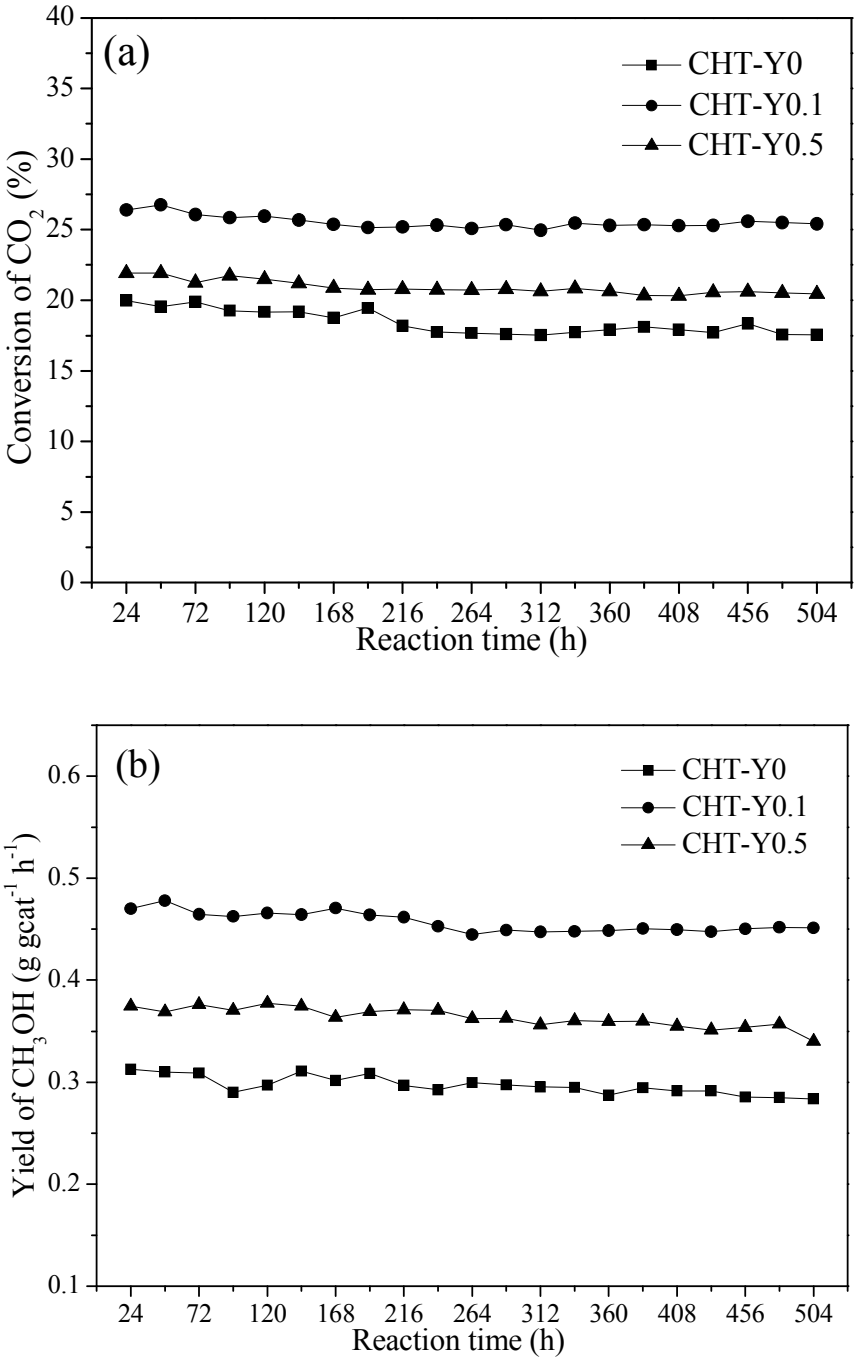

Fig. 10. The trend of (a) CO_2 conversion and (b) CH_3OH yield versus reaction time over CHT-Y0 (rectangles), CHT-Y0.1 (circles) and CHT-Y0.5 (triangles) catalysts. Reaction conditions: T=523 K, P = 5.0 MPa, GHSV = 10,000 mL $gcat^{-1}$ h^{-1}, $H_2/CO_2/N_2$= 73/24/3 (molar ratio).

Catalysis Science & Technology Accepted Manuscript

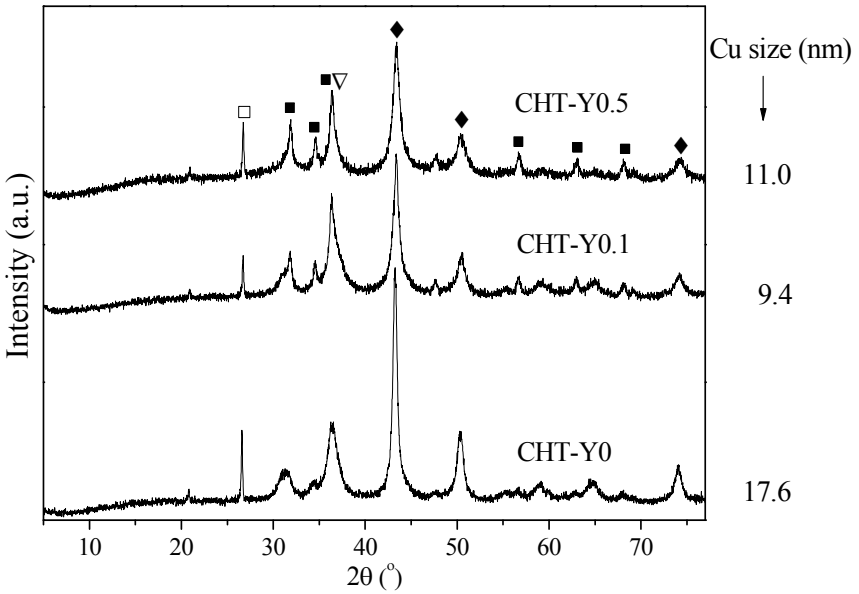

Fig. 11. XRD patterns of spent CHT-Y0, CHT-Y0.1 and CHT-Y0.5 catalysts after 500 h. (◆)Cu; (▽) Cu_2O; (■) ZnO; (□) SiO_2. Peaks for SiO_2 in each spent sample came from residue quartz sand used for catalyst dilution.

Catalysis Science & Technology Accepted Manuscript